Journal of Molecular Structure 1294 (2023) 136389

Contents lists available at ScienceDirect

Journal of Molecular Structure

journal homepage: www.elsevier.com/locate/molstr

Vibrational spectroscopy of neutral and cationic 2-Methoxyethanol

Xiaohu Zhou [a], Ende Huang [a,b], Licheng Zhong [a], Siyue Liu [a,c], Shuze Ma [a,b], Hongwei Li [a], Xueming Yang [a,d,e], Wenrui Dong [a,e,*]

[a] State Key Laboratory of Molecular Reaction Dynamics, Dalian Institute of Chemical Physics, Chinese Academy of Sciences, Dalian, 116023, China
[b] University of Chinese Academy of Sciences, Beijing, 100049, China
[c] Key Laboratory of Materials Modification by Laser, Ion, and Electron Beams, Chinese Ministry of Education, School of Physics, Dalian University of Technology, Dalian 116024, China
[d] Department of Chemistry, Southern University of Science and Technology, Shenzhen, 518055, China
[e] Hefei National Laboratory, Hefei, 230088, China

ARTICLE INFO

Keywords:
Gas phase infrared spectroscopy
Intramolecular hydrogen bond
Molecular structure
NBO analysis
Negative hyperconjugation

ABSTRACT

Hydrogen bonding interactions, such as the O-H···O interaction, play a crucial role in stabilizing conformations of both organic and biological molecules. In this study, we employed the infrared (IR)–vacuum-ultraviolet (VUV) non-resonant ionization detected IR spectroscopy (NRID-IR) method to investigate the molecular structure of neutral and cationic 2-methoxyethanol ($CH_3OCH_2CH_2OH$, 2-ME). The stable structures and anharmonic IR spectra of neutral and cationic 2-ME were calculated using density functional theory (DFT) at the B3LYP-D3(BJ)/def2-TZVPP level. Our results revealed that the two most stable conformers of neutral 2-ME exhibit a weak O-H···O intramolecular hydrogen bond, while the cationic 2-ME lacks the O-H···O interaction but contains a C-H···O intramolecular hydrogen bond. A comparison of the experimental and theoretical IR absorption spectra reveals that the most stable conformer (gauche-(anti-gauche)-trans) is the primary contributor to the observed IR spectra of neutral 2-ME in the 2700–7250 cm^{-1} range. Similarly, the second stable conformer is found to be the dominant contributor to the observed IR spectra of cationic 2-ME in the range of 2700–7100 cm^{-1}. Additionally, the C-H fundamental stretching mode of cationic 2-ME is found to be blue-shifted by approximately 100 cm^{-1} compared to that of neutral 2-ME. Furthermore, the natural bond orbital (NBO) analysis suggests that in neutral 2-ME, the $n(O)\rightarrow\sigma^*(C_\alpha H)$ interactions result in significant negative hyperconjugation, leading to the weakening of $C_\alpha H$ bonds and a subsequent reduction in vibrational energy.

1. Introduction

Because of its importance in the molecular structure, function, and dynamics of organic, inorganic, and biological chemistry, hydrogen bonding is a critical area of research [1–3]. In nature, there are two types of hydrogen bonding interactions: inter- and intra-molecular hydrogen bonding interactions. Alcohols are frequently employed as model molecules for investigating the inter- and intra-molecular hydrogen bonds due to the high sensitivity of their OH stretching vibrational frequency to these interactions [4–7].

2-Methoxyethanol ($CH_3OCH_2CH_2OH$, 2-ME), an exemplary ether alcohol, has received massive attention as a valuable model compound for investigating inter- and intra-molecular hydrogen bonding interactions [8–12,5,13,14]. Brinkley et al.[5] studied the impact of concentration and temperature on the intra- and inter-molecular hydrogen bonding of 2-ME in *n*-hexane. Their findings indicate that the intermolecular hydrogen bonding interaction is stronger than the intramolecular counterpart; at elevated temperatures (318 K), the hydrogen bonding in 2-ME is weakened due to the increased thermal energy. Jiang et al.[15] reported that the O-H···O hydrogen bond between the ether oxygen of 2-ME and the surface hydroxyl group of TiO_2 enhances visible light absorption, thereby promoting the visible light photocatalytic activity of TiO_2. Furthermore, owing to its unique physicochemical properties, 2-ME has found extensive use as a solvent and chemical intermediate. For example, it has been identified as a solvent for large-area perovskite film coating due to its low boiling point and high vapor pressure [16–19]. In addition, the presence of an O-CH_2-CH_2-O group in 2-ME makes it crucial for understanding the structural dynamics of poly (oxyethylene) crown ether [10].

Previous IR spectroscopic studies on 2-ME have primarily focused on

* Corresponding author.
E-mail address: wrdong@dicp.ac.cn (W. Dong).

https://doi.org/10.1016/j.molstruc.2023.136389
Received 1 June 2023; Received in revised form 2 August 2023; Accepted 8 August 2023
Available online 8 August 2023

the liquid phase [8,11,12,5] or the lower frequency range (800–1500 cm^{-1}) during Ar matrix isolation experiments conducted at low temperatures (11-44 K) [10]. Fourier transform infrared (FTIR) spectroscopy studies have revealed that the gauche-(anti-gauche)-trans conformation was dominated in the liquid phase, with a minor contribution from the less stable trans-trans-trans conformation, which lacks intramolecular hydrogen bonding interactions [8,12]. Yoshida et al.[10] measured the IR spectra of 2-ME in an argon matrix at temperatures from 11 to 44 K, demonstrating the presence of only the gauche-(anti-gauche)-trans conformation, which is stabilized by intramolecular hydrogen bonding interactions. It is expected that the distribution of conformers in the gas phase would differ due to the higher internal energy that can be attained at room temperature.

The VUV laser is commonly employed as a highly effective soft ionization source for molecules and clusters. This is particularly advantageous under near-threshold ionization conditions, as it avoids complications arising from fragmentation. By combining the supersonic jet technique with time-of-flight mass spectrometry (TOF-MS) and a tunable VUV light source, the resulting IR-VUV spectroscopy enables size-selected and conformer-specific analysis. This approach facilitates a more reliable investigation of the geometric structures and ionization dynamics of molecules, clusters, and radicals. Notably, this method has found extensive application in the study of neutral and cationic molecular monomers and clusters, including water [20,21], alcohols [22,23], ammonia, [24,25] acetone, [26,27] and pyridine [28].

In this study, we employed the non-resonant ionization detected IR spectroscopy (NRID-IR) method to measure the vibrational spectra of neutral and cationic 2-ME. This was achieved by monitoring the changes in the ionic signal intensity for the fragment ($m/z = 45$) and the parent ($m/z = 76$) upon resonance absorption of IR radiation. By comparing the experimentally observed IR spectra with those simulated using DFT calculations, we proposed the dominant spectral carriers for both neutral and cationic 2-ME. Furthermore, we investigated the structural differences between neutral and cationic 2-ME using electron density distribution calculation.

2. Methodology

2.1. Experimental section

The IR absorption spectra of the neutral and cationic 2-ME molecules were obtained by monitoring the changes in the ionic signal of 2-ME ($m/z = 76$) and its dissociative ionization fragment $[C_2H_5O]^+$ ($m/z = 45$) while scanning the frequency of the IR laser arriving before or after the VUV laser. The 118 nm VUV laser was generated by frequency tripling the 355 nm laser (40 mJ $pulse^{-1}$), which is the triple frequency of the output of a Nd: YAG laser (Beamtech, SGR-20, 10 Hz). The 118 nm laser was generated in a cell containing a gaseous mixture of Xe and Ar (Xe: Ar = 1:10) at a total pressure of approximately 300 Torr. A convex MgF_2 lens was mounted at the end of the gas cell to focus the 118 nm laser into the center of the ionization region.

The tunable IR radiation was generated using an optical parametric oscillator/amplifier (OPO/OPA) system (Laser Vision) with a resolution of 0.9 cm^{-1} in broadband mode. The OPO/OPA system was pumped by the 1064 nm output of an injection-unseeded Nd: YAG laser (Continuum, Surelite EX) operating at a repetition rate of 5 Hz with a pulse energy of 630 mJ. The IR laser, with a typical energy of 10 mJ per pulse at the entrance of the CaF_2 window, was focused into the ionization region using a CaF_2 lens ($f = 500$ mm).

At a back pressure of 25 psi, Helium was passed through a bubbler containing anhydrous 2-ME (99.8%, Sigma-Aldrich) at room temperature (vapor pressure is about 10 Torr). The molecular beam, consisting of approximately 1% 2-ME in helium, was generated using a pulsed solenoid valve (Parker, General Valve Series 9) with a 0.5 mm orifice operating at a repetition rate of 10 Hz. The molecular beam was collimated by a 1.5 mm diameter skimmer located approximately 2 cm downstream of the pulsed nozzle. Subsequently, it intersected perpendicularly with the VUV (118 nm) laser in the ionization region.

The IR laser was counter-propagated with the VUV laser, and the two laser beams overlapped in the ionization region. For the measurement of the neutral 2-ME IR spectrum, the IR laser was set to arrive 50 ns before the VUV laser, while for the measurement of the cationic 2-ME IR spectrum, the IR laser was set to arrive 50 ns after the VUV laser. The ion signal was amplified using an amplifier (Stanford Research Systems, SR445A) and then fed to a digital storage oscilloscope (InfiniiVision DSO-X 3054A) before being recorded by a computer. The IR spectra were obtained by subtracting the background ion signal from the VUV single-photon ionization (IR on - IR off).

2.2. Computational section

To determine the lowest energy structure of the 2-ME molecule, automated conformational searches were initially conducted using the Molclus program [29]. Subsequently, the 27 searched structures underwent preliminary geometry optimizations using density functional theory (DFT) with Grimme's dispersion correction, Becke-Johnson damping, and three-body terms D3(BJ) [30–32] at the B3LYP/def2-SVP level, utilizing the Gaussian 16 program suite [33]. The resulting 12 stable conformers of 2-ME were further reoptimized at the B3LYP-D3(BJ)/def2-TZVPP level. Similarly, seven distinct structures of cationic 2-ME were identified.

The vibrational analysis of both the neutral and cationic 2-ME structures was performed at the B3LYP-D3(BJ)/def2-TZVPP level to obtain the zero-point energies (ZPE). Single-point energy calculations were carried out at the RIJK-CCSD(F12*)(T*)/cc-pVTZ-F12//B3LYP-D3(BJ)/def2-TZVPP level using the ORCA program, with a ZPE correction [34].

Mayer bond order analysis was performed using the Multifunctional Wavefunction Analyzer (Multiwfn) program [35], based on the wavefunction obtained from the Gaussian 16 program. The interaction region indicator (IRI) approach and the electron density distribution of the highest occupied orbitals of the neutral 2-ME were calculated at the B3LYP/def2-SVP level. Visualization analysis was performed using the Multiwfn and Visual Molecular Dynamics (VMD) programs [36].

The anharmonic IR absorption spectra of both the neutral and cationic 2-ME were simulated using the vibrational second-order perturbation theory (VPT2) approach, implemented in the Gaussian 16 programs, at the B3LYP-D3(BJ)/def2-TZVPP level of theory.

To determine the gas-phase acidity (ΔG_{acid}) of the CH bonds in both the neutral and cationic 2-ME, the change in Gibbs energy during the following reactions was considered: $CH_3OCH_2CH_2OH \rightarrow CH_2OCH_2CH_2OH^- + H^+$ and $CH_3OCH_2CH_2OH^+ \rightarrow CH_2OCH_2CH_2OH^\bullet + H^+$. The energies of $CH_3OCH_2CH_2OH$, $CH_2OCH_2CH_2OH^-$, $CH_3OCH_2CH_2OH^+$, and $CH_2OCH_2CH_2OH^\bullet$ were calculated at the B3LYP-D3(BJ)/def2-TZVPP level of theory, accounting for the ZPE correction. The gas-phase acidity was evaluated at a temperature of 298.15 K.

3. Results and discussion

3.1. Structure of neutral and cationic 2-ME

Neutral 2-ME. The HOCC, OCCO, and CCOC torsions of the 2-ME molecule each have three non-trivial torsion angles (or dihedral angles), which in turn exist in trans, gauche, and anti-gauche forms, denoted as (T, t), (G, g), and (G′, g′), respectively. Consequently, there are a total of 27 possible rotamers for 2-ME. In this work, we adopted the nomenclature proposed by Gawrilow et al.[14], where lowercase letters (t, g, g′) represent the HOCC torsion angles, and uppercase letters (T, G, G′) represent those of the OCCO and CCOC torsion angles. The corresponding torsion angle ranges are as follows: $0 \leq (G', g') \leq 120^\circ \leq (T, t) \leq 240^\circ \leq (G, g) \leq 360^\circ$

Quantum chemical calculations revealed that 12 of the 27 conformers are stable, consistent with previously calculated results by Abdel-Rahman et al. [37] and Gawrilow et al.[14]. The structures of these 12 stable conformers, along with their relative energies (ΔE), are shown in Fig. S1 (Supporting Information). Among them, the gG′T conformer exhibits the lowest energy and is therefore expected to be the most stable conformer of 2-ME. Its optimized structure, with certain pivotal bond lengths and angles labeled, is shown in Fig. 1a. The next most stable conformer, gG′G′, is 1.44 kcal mol^{-1} higher in energy than gG′T.

Furthermore, the Boltzmann distribution was calculated for temperatures ranging from 0 to 350 K, as summarized in Table S1. It is evident that the gG′T conformer is expected to dominate over the other conformers at temperatures below room temperature, with the Boltzmann weight of gG′T exceeding 80%.

Cationic 2-ME. Six out of seven stable conformers of cationic 2-ME have relative energies within a 2 kcal mol^{-1} window, with the optimized structure of the most stable conformer depicted in Fig. 1b. The next most stable conformer is less than 1 kcal mol^{-1} higher in energy compared to the global minimum structure. The optimized structures of seven stable conformers of cationic 2-ME, along with their relative energies, are presented in Fig. S2. The optimized structure of cationic 2-ME differs from that of neutral 2-ME (shown in Fig. 1a and 1b) in several aspects, namely, the hydroxyl hydrogen is oriented away from the ether oxygen; the O1-C3 bond length was shortened from 1.42 Å to 1.34 Å, accompanied by an elongation of C3-C4 bond from 1.51 Å to 1.71 Å. Consequently, the Mayer bond order of C3-C4 decreases from 0.96 to 0.67 (at the B3LYP/def2-TZVPP level). This suggests that, when the internal energy of cationic 2-ME is sufficient, the C3-C4 bond tends to break, leading to the formation of CH_2OH and $[C_2H_5O]^+$ (m/z = 45). The substantial contrast between the neutral and cationic configurations implies that the ion produced during vertical ionization is unstable and is expected to undergo isomerization to the stable cationic configuration without encountering an energy barrier. The appearance energy (AE) of this channel is 10.36 eV, [39] slightly higher than the ionization energy (IE) of 2-ME (10.13 eV) [40]. Thus, IR spectroscopy can be obtained by monitoring the variation of the $[C_2H_5O]^+$ signal as the IR wavelength is scanned, with the IR pulses before (for the IR spectra of neutral 2-ME) or after (for the IR spectra of cationic 2-ME) the VUV laser.

Previous studies have suggested that the stability of neutral 2-ME

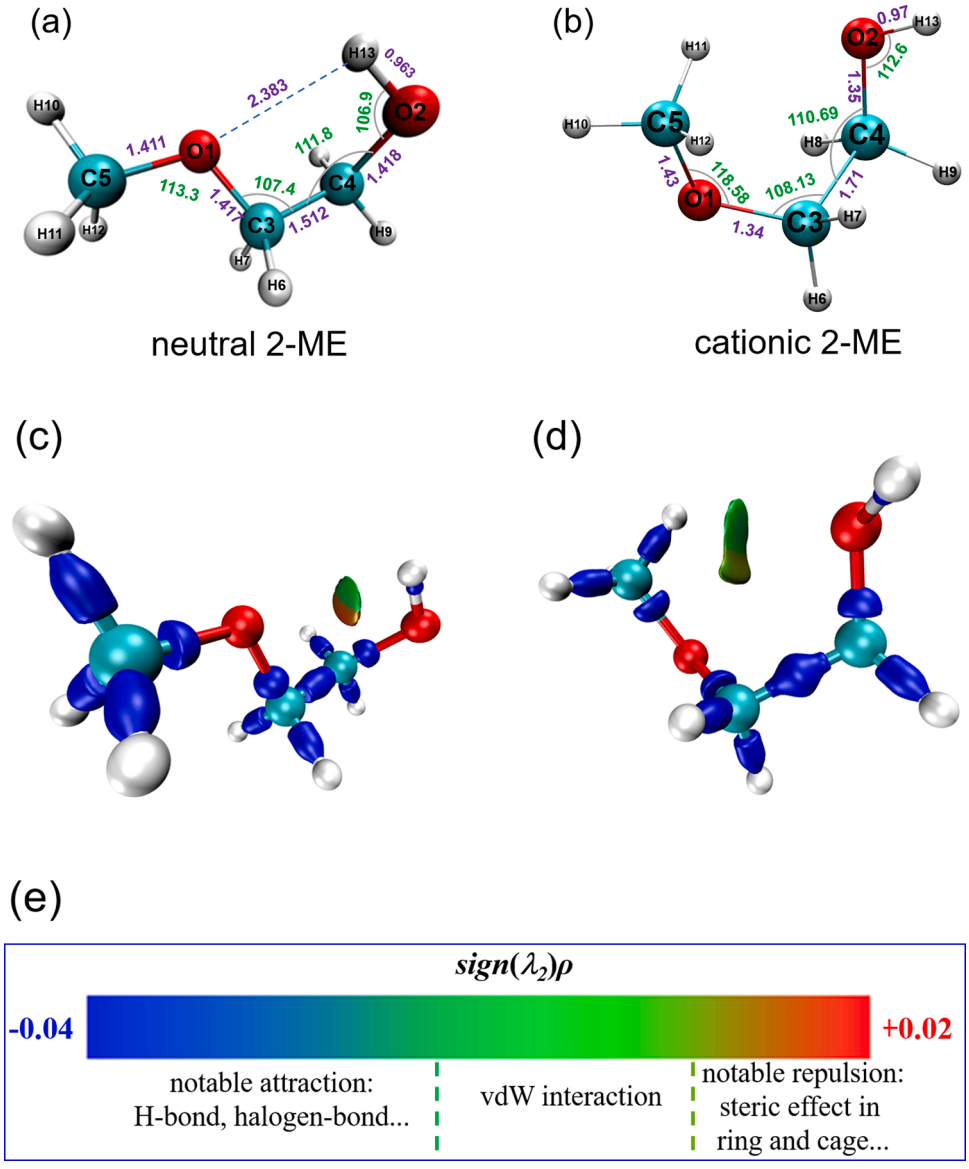

Fig. 1. Optimized most stable structure of neutral (a) and cationic (b) 2-ME (pivotal bond lengths and bond angles are labeled). Isosurface map of IRI=1.1 of neutral (c) and cationic (d) 2-ME. *sign*(λ_2)ρ is mapped on the isosurfaces according to the coloring method of (e) [38].

and tetrahydropyran-2 methanol is influenced by an intramolecular hydrogen bond between the ether oxygen and hydroxy group of the CH_2OH group [37,41]. To assess the strength of this intramolecular hydrogen bond, the interaction region indicator (IRI) approach was used to analyze weak interactions in neutral 2-ME. The IRI is a new real-space function that slightly modifies the reduced density gradient (RDG) [38]. Similar to the noncovalent interaction (NCI) method, [42] the $sign(\lambda_2)\rho$ function was mapped onto the IRI isosurface using different colors to represent both covalent and noncovalent interactions. Here, sign(λ_2) represents the sign of the second largest eigenvalue (λ_2) of the electron density (ρ) Hessian matrix, which can be used to distinguish attractive and repulsive interactions [42]. The IRI maps of neutral and cationic 2-ME are shown in Fig. 1c and 1d, respectively, using the coloring method shown in Fig. 1e. The IRI map of neutral 2-ME reveals an intramolecular hydrogen bond between the ether oxygen and the terminal hydroxy group of CH_2OH. Due to the relatively long hydrogen bond (2.38 Å) and the large bending degree of O2-H13···O1 (see Fig. 1a), the strength of the hydrogen bond is weak and similar to the van der Waals interaction. However, this weak hydrogen bond plays a crucial role in stabilizing 2-ME, as evidenced by the fact that the energy of conformer gGT (where the terminal OH is rotated by 120° relative to conformer gG′T, resulting in no bond formation between H13 and O1) is more than 2.91 kcal mol^{-1} higher than that of conformer gG′T (see the corresponding relative energies of conformer gG′T and gGT in Fig. S1), and that the second most stable conformer of gG′G′ also contains a weak hydrogen bond (O2-H13···O1). The weak intramolecular hydrogen bond (O2-H13···O1) is broken when an electron is removed from the nonbonding *p*-orbital of the oxygen atom at the ether linkage while forming the cationic 2-ME. The IRI map of cationic 2-ME shows a particularly weak C-H···O hydrogen bond between the C5-H11 of the CH_3 group and the O atom of the hydroxy group. Previous studies have shown that intramolecular C-H···O interactions are important [43,44] and compete with the commonly accepted intramolecular hydrogen bonds such as O-H···O and O-H···S [45,46]. The calculated gas-phase acidity (ΔG_{acid}) of cationic 2-ME is 200.6 kcal mol^{-1} (at 298.15 K), which is 207.1 kcal mol^{-1} lower than that of neutral 2-ME. This indicates an enhanced ability to donate protons from the C5-H11 bond in the cationic form, leading to an increased electrostatic attraction between H11 and the negatively charged O atom and the formation of a weak C—H···O hydrogen bond.

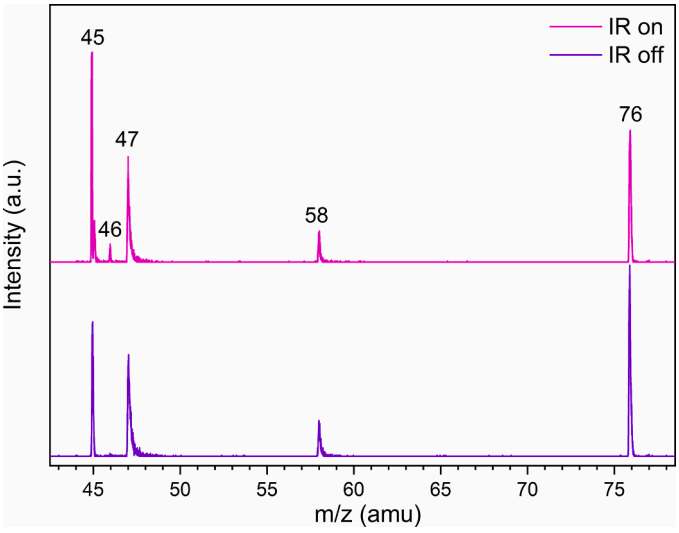

Fig. 2. Mass spectra of 2-ME and its fragmentation products obtained by single-photon ionization at 118 nm, with the presence (2940 cm^{-1}, top panel) or absence (bottom panel) of an IR laser.

3.2. VUV photoionization mass spectra of 2-ME

Fig. 2 shows the mass spectra of 2-ME and its fragmentation products obtained by single-photon ionization at 118 nm (10.5 eV) with (pink) and without (purple) the IR radiation at 2940 cm^{-1}. The ionization energy (IE) of 2-ME and the AE of its fragments are provided in Table 1. The dominant fragment is $[C_2H_5O]^+$ ($m/z = 45$), which arises from the cleavage of the C3-C4 bond of the 2-ME cation, accompanied by the co-product CH_2OH. Holmes et al.[47] proposed that $[CH_3O(H)CH_2]^+$ serves as the carrier for the $m/z = 46$ peak, as the hydroxyl hydrogen is transferred to the ether oxygen atom prior to the cleavage of the C3-C4 bond. On the other hand, Burgers et al.[48] suggested that it is $[CH_2{=}CH{\cdots}H{\cdots}OH_2]^+$, based on the experiment with partially deuterated 2-ME. The cationic 2-ME can decompose into formaldehyde ($H_2C{=}O$) and the O-protonated methoxymethyl radical, which features a proton bridge between the two entities. This radical abstracts a hydrogen atom from the formaldehyde before decomposing into HCO and $[(CH_3)_2OH]^+$ ($m/z = 47$) [49]. Furthermore, the cationic 2-ME can generate $[C_3H_6O]^+$ ($m/z = 58$) and H_2O, as the hydrogen atom from either the methyl or the β-methylene group is transferred to the terminal OH prior to the breaking of the C—O bond [50,51].

Figure 2 illustrates that the introduction of the IR laser (2940 cm^{-1}, 0.37 eV) into the ionization region 50 ns prior to the VUV laser (118 nm, 10.5 eV) resulted in a decrease in the signal of $m/z = 76$ and an increase in the signal of $m/z = 45$. This can be attributed to the higher total energy (10.9 eV compared to 10.5 eV) absorbed by 2-ME, which enhanced its dissociative ionization efficiency.

3.3. IR spectra of neutral 2-ME

The IR-VUV non-resonant ionization and fragmentation detected (NRIFD-IR) vibrational spectra of neutral 2-ME follows a similar principle as that of methanol, ethanol, acetone, acetic acid [23,27,53,54]. Fig. 3 shows the observed and calculated IR spectra of neutral 2-ME in the wavenumber range of 2700–7250 cm^{-1}. Specifically, Fig. (3a) and (3b) display the IR dip and IR enhancement spectra, respectively, obtained by monitoring the parent cation $m/z = 76$ mass channel and its fragment cation $m/z = 45$ mass channel. Additionally, Fig. (3c-e) depict the calculated anharmonic (VPT2) IR spectra at the B3LYP-D3 (BJ)/def2-TZVPP level of theory for the three most stable conformers of 2-ME. Among these conformers, two involve an intramolecular hydrogen bond (gG′T and gG′G′), while the C-O-C-C-O of the third conformer lies in the same plane (tTT). Due to the lower signal-to-noise ratio of the IR dip spectra, our discussion primarily focuses on the results obtained from the enhancement spectra.

In the 2700–3100 cm^{-1} region, we observed a broadband featuring two strong peaks centered at approximately 2898 and 2933 cm^{-1}, along with three shoulder peaks centered at around 2840, 2959, and 2974 cm^{-1} (for detailed information, see Fig. S3a in the Supporting Information). Fig. 3 demonstrates that the simulated IR spectra of the most stable conformer, gG′T, exhibit better agreement with the experimental results in this region. Additionally, Fig. S3b shows several simulated vibrational modes with integrated intensity >1 km mol^{-1} in the 2700–3100 cm^{-1} range. The calculated vibrational frequencies and intensities of these modes can be found in Table S2 in the Supporting Information. Among seven fundamental CH stretching transitions (from ν_2

Table 1
The ionization energy (IE) of 2-ME and appearance energy (AE) of its fragments.

Ion	Product	IE/AE (eV)
$m/z = 76$	$[CH_3OCH_2CH_2OH]^+$	10.13 [40]
$m/z = 45$	$[C_2H_5O]^+ + CH_2OH$	10.36 [39]
$m/z = 46$	$[C_2H_6O]^+ + CH_2O$	10.30 [48]
$m/z = 47$	$[C_2H_7O]^+ + HCO$	9.96 [52]
$m/z = 58$	$[C_3H_6O]^+ + H_2O$	/

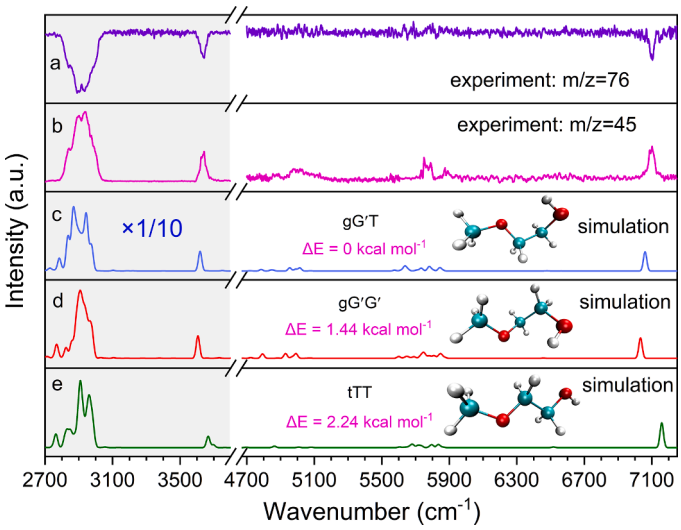

Fig. 3. Observed IR spectrum of neutral 2-ME in the 2700–7250 cm^{-1} region (the 2700–3800 cm^{-1} region is compressed by a factor of ten) obtained by monitoring the parent cation of the $m/z = 76$ mass channel (Fig. 3a) and its fragment cation of $m/z = 45$ mass channel (Fig. 3b). The optimized structures and simulated anharmonic IR spectra (VPT2) of the three most stable conformers are shown in (Fig. 3c-e). The simulated anharmonic IR spectra were obtained by convoluting the simulated IR stick spectra (Fig. S3 in the Supporting Information) with a Gaussian profile (24 cm^{-1} FWHM). The calculations were performed at the B3LYP-D3(BJ)/def2-TZVPP level. The relative ZPE-corrected energies of the three conformers are also provided.

to ν_8), the four highest frequencies correspond to antisymmetric modes (two for the CH_3 group and one for each CH_2 group), while the three lowest frequencies are assigned to the symmetric modes of CH_3 and two CH_2 stretching, respectively. Furthermore, the modes from ν_9 to ν_{13} are attributed to the CH_3 bending vibrations.

Accurate assignment of these absorption peaks is challenging due to the complexity of the predicted IR spectra and the broad experimental spectra. After careful comparative analysis, the shoulder feature at approximately 2840 cm^{-1} can be assigned to the sum contribution of CH_2 symmetric stretching (ν_6 and ν_8). Previous studies on tetrahydrofuran (C_4H_8O) have reported that the stretching frequencies of the $C_\alpha H$ (the first carbon atom attached to the oxygen atom) are lower than those of the $C_\beta H$ (the second carbon atom attached to the oxygen atom) [55]. This observation was attributed to the negative hyperconjugation [56–59] between the $C_\alpha H$ bonds and the nonbonding orbital of the oxygen atom. In the case of 2-ME, the frequencies of the two CH_2 symmetric stretching modes (ν_6 and ν_8) show no noticeable difference. This can be explained by the presence of negative hyperconjugations between the CH bonds of the two CH_2 groups and the nonbonding orbitals of the two oxygen atoms.

The feature centered at approximately 2898 cm^{-1} is tentatively assigned to the sum contribution of CH asymmetric stretching for the CH_2 group ν_5, combination bands of $\nu_{13} + \nu_{11}$ and $\nu_{13} + \nu_{12}$, and overtone bands of $2\nu_{12}$ and $2\nu_{13}$. The feature centered at around 2933 cm^{-1} is attributed to the sum contribution of ν_3, $2\nu_{10}$, $\nu_{11} + \nu_9$, and $\nu_{10} + \nu_9$. The two shoulder features at approximately 2959 and 2974 cm^{-1} are attributed to the overtone of the CH_3 bending vibration mode ($2\nu_9$) and the CH antisymmetric stretching of CH_3 (ν_2), respectively. The observed IR spectrum in the 2700–3100 cm^{-1} region closely resembles the FTIR spectra obtained in the liquid phase [11]. In these spectra, five bands were observed, centered at 2828, 2882, 2895, 2931, and 2980 cm^{-1}.

As shown in Fig. 3a, one broadband and two peaks were observed in the 4900–5100 cm^{-1} and 5600–5900 cm^{-1} regions, respectively. The detailed assignments of these bands are presented in Fig. S4. The feature in the 4900–5100 cm^{-1} region consists of two bands centered at approximately 4975 cm^{-1} and 5015 cm^{-1}. According to the simulated spectra from gG′T, these bands can be attributed to the combination of COH bending vibration (δ_{COH}) with OH stretching vibration ($\nu_{16} + \nu_1$), and the combination of C-C stretching vibration with OH stretching vibration ($\nu_{14} + \nu_1$), respectively. Three features centered at approximately 5750, 5789, and 5875 cm^{-1} originate from overtones of CH_3 and CH_2 stretching modes ($2\nu_{CH}$ region), specifically the CH_3 antisymmetric stretching overtone $2\nu_4$, CH_2 antisymmetric stretching overtone $2\nu_3$, and CH_3 antisymmetric stretching overtone $2\nu_2$. Two weaker peaks at 5735 and 5891 cm^{-1} are assigned to the ($\nu_8 + \nu_4$) and ($\nu_4 + \nu_2$) combination bands, respectively.

The sharp and intense peak centered at approximately 3635 cm^{-1} corresponds to the fundamental OH stretching region (ν_1). The OH stretching vibration can be categorized into three types: free (unbonded) OH stretching, intramolecular hydrogen-bonded OH stretching, and intermolecular hydrogen-bonded OH stretching. In the gas phase, intramolecular hydrogen bonding dominates over the intermolecular intramolecular hydrogen-bonded OH stretching and vice versa for the liquid phase, in which the vibration of the free OH stretching is negligible [5]. Our DFT calculations predicted that the OH stretches of gG′T (3619 cm^{-1}) and gG′G′ (3606 cm^{-1}) are red-shifted by about 48 and 61 cm^{-1}, respectively, compared to the tTT conformer (3667 cm^{-1}, which exhibits free OH stretching due to the absence of a hydrogen bond). The observed peak at 3635 cm^{-1} is red-shifted from the free OH stretch of gas-phase alcohols (3665–3682 cm^{-1}) [22,53], and we tentatively assign it to the intramolecular hydrogen-bonding stretch. This assignment is supported by the fact that the measured intramolecular hydrogen-bonding stretch of tetrahydropyran-2-methanol (3614 cm^{-1}) [41], which contains both ether oxygen and hydroxyl groups, is close to that of 2-ME (3635 cm^{-1}).

The calculated frequencies from ν_1 for different conformers, gG′G′ (3606 cm^{-1}), gG′T (3619 cm^{-1}), and tTT (3667 cm^{-1}), indicate that the OH stretch frequency decreases with an increasing number of gauche arrangements. The feature at approximately 7095 cm^{-1} is assigned to the first overtone of the OH stretch ($2\nu_1$). The predicted frequencies of $2\nu_1$ are 7060, 7033, and 7159 cm^{-1} for gG′T, gG′G,′ and tTT conformers, respectively.

In the supersonic molecular beam, neutral 2-ME is dominated by the gG′T conformer, as the simulated IR spectra of the gG′T conformer closely match the experimental one. The gG′G′ conformer, which exhibits a similar intramolecular hydrogen bonding structure, is energetically higher by 1.44 kcal mol^{-1} compared to the gG′T conformer.

3.4. IR spectra of cationic 2-ME

The IR spectra of cationic 2-ME were obtained using a method similar to that of neutral 2-ME, with the exception that the IR pulse was fired 50 ns after the VUV radiation. The measured IR spectra, obtained by monitoring the variation of the $m/z = 45$ and $m/z = 76$ signals upon the IR radiation, are shown in Fig. 4a and 4b, respectively. The simulated IR spectra of the two most stable conformers of the 2-ME cation are presented in Fig. 4c-d. These spectra were obtained by convoluting the simulated IR stick spectra (Fig. S5-S6 in the Supporting Information) with a Gaussian profile (24 cm^{-1} FWHM).

Similar to the IR spectra of neutral 2-ME, the cationic spectra also exhibit a broad band between 2800 and 3100 cm^{-1} in the ν_{CH} region. This band is characterized by a strong peak centered at around 2979 cm^{-1} and four shoulder features at about 2945, 2992, 3033, and 3069 cm^{-1} (Fig. S5a in the Supporting Information). The predicted stick spectrum of the C2 conformer (Fig. S5b in the Supporting Information) includes seven CH stretch fundamental vibrations (modes from ν_2 to ν_8), four combination bands ($\nu_{11} + \nu_{10}$, $\nu_{10} + \nu_9$, $\nu_{33} + \nu_8$, $\nu_{33} + \nu_5$), and two overtone bands ($2\nu_9$, $2\nu_{11}$). Although other combination and overtone bands have been predicted in this energy range, none exhibits significant IR intensity. Based on the calculated IR frequency and relative intensity (Table S3 in the Supporting Information), the strong peak at about 2979 cm^{-1} is assigned to the antisymmetric CH_3 stretching (ν_5), the 2945

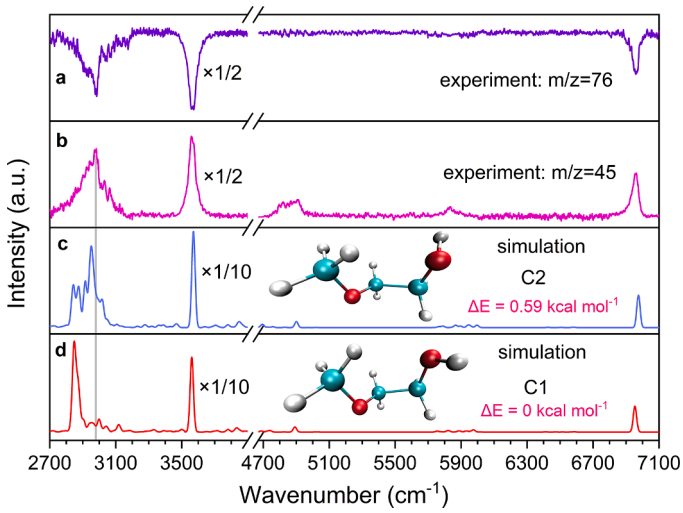

Fig. 4. Observed IR spectrum of cationic 2-ME in the 2700–7100 cm^{-1} region (ν_{OH} region are compressed by a factor of two) obtained by monitoring the parent cation of the $m/z = 76$ mass channel (Fig. a) and its fragment cation of the $m/z = 45$ mass channel (Fig. b). The optimized structure and simulated anharmonic IR spectra (VPT2) of the two most stable conformers of cationic 2-ME (ν_{OH} region is compressed by a factor of ten) are shown in Fig. c and d. The structures and spectra were obtained at the B3LYP-D3(BJ)/def2-TZVPP level. The calculated IR spectra were generated by convoluting the stick spectra (Figs. S5-S6) with a Gaussian profile (24 cm^{-1} FWHM). The relative ZPE-corrected energies of the two conformers are also provided.

cm^{-1} feature is assigned to the combination band of $\nu_{10} + \nu_9$, which arises from CH_3 and CH_2 bending vibrations, and the weaker band at about 2992 cm^{-1} arises from the antisymmetric CH_2 stretching (ν_4). The two weaker bands at 3033 and 3069 cm^{-1} are assigned to antisymmetric CH_2 (ν_3) and CH_3 (ν_2) stretching, respectively. Additionally, a sharp peak centered at 3560 cm^{-1} corresponds to the fundamental OH stretching vibration. The broader bandwidth observed in the cationic IR spectrum compared to the neutral spectrum suggests that the cationic 2-ME may possess a higher temperature due to the excess energy acquired during the ionization process. This behavior is consistent with the previously reported IR spectra of neutral and cationic ethanol [53]. It is worth noting that the OH vibrational frequency of cationic 2-ME is redshifted by 75 cm^{-1} relative to that of neutral 2-ME, and the origin of this shift will be discussed in Section 3.5.

In the frequency range of 4600–7000 cm^{-1}, two broad bands were observed at 4750–4950 and 5785–5885 cm^{-1}. Three features centered at 4795, 4821, and 4908 cm^{-1} (labeled in Fig. S6) are attributed to the combination bands of the $\nu_{19} + \nu_1$, $\nu_{18} + \nu_1$, and $\nu_{14} + \nu_1$ transitions, respectively. The weak broadband observed between 5785 and 5865 cm^{-1}, with a centered at 5825 cm^{-1}, is mainly contributed by the combination bands of CH stretching. Additionally, the sharp peak at 6958 cm^{-1} is undoubtedly assigned to the first overtone stretching vibration of OH ($2\nu_1$).

The simulated IR spectra of the C2 conformer exhibit better agreement with the experimental spectra, particularly in the CH fundamental stretching region. Despite the C1 conformer being energetically favored over the C2 conformer by 0.59 kcal mol^{-1}, as determined by the RIJK-CCSD(F12*)(T*)/cc-pVTZ-F12//B3LYP-D3(BJ)/def2-TZVPP level of theory, the dominance of the C2 conformer in the cationic 2-ME can be attributed to the distribution of a portion of the excess energy (about 0.37 eV, considering that 2-ME is ionized by 118 nm laser and its IE is 10.13 eV) to the internal energy of the 2-ME cation.

3.5. Comparison of IR spectra between neutral and cationic 2-ME

To investigate the orbital from which an electron was removed during photoionization, a molecular orbital (MO) analysis of neutral 2-ME was conducted at the B3LYP/def2-TZVPP level. The highest occupied molecular orbital (HOMO) of neutral 2-ME, as shown in Fig. 5a, is primarily localized on the oxygen atom at the ether linkage (O1). Its electron densities in this orbital are predominantly associated with the oxygen lone pair orbital (n(O)), with contributions from the *p* orbitals of the neighboring carbon atoms (C3 and C5), and a negligible contribution from n(O2). Consequently, the removal of an electron from the HOMO weakens the adjacent C3-C4 bond, resulting in an elongation of the C3-C4 bond length from 1.51 to 1.71 Å. This increased bond length renders the C3-C4 bond susceptible to cleavage, thereby explaining the dominance of the $[C_2H_5O]^+$, as shown in Fig. 2. In contrast, the ionization process has a minimal impact on the OH stretching due to the limited contribution of the n(O2) nonbonding electrons to the HOMO. Consequently, the OH vibrational frequency of the 2-ME cation experiences only a modest redshift of approximately 75 cm^{-1} relative to that of the neutral 2-ME. This behavior differs significantly from ethanol, where the HOMO is located on the n(O) orbital of the OH group. In the case of ethanol, the OH vibrational frequency of the cation undergoes a redshift of over 200 cm^{-1} compared to that of neutral ethanol [53]. The discrepancy arises from the fact that the electron loss from the nonbonding *p* orbital of the oxygen atom in cationic ethanol imparts chemical similarity to the N atom, thereby reducing the energy associated with the OH stretching [60].

The experimental results reveal a blueshift of about 100 cm^{-1} in the C—H stretching bands of cationic 2-ME compared to the neutral 2-ME. This observation is unexpected, as the removal of an electron from the HOMO would typically result in a slight weakening of the C—H (C3 and C5) stretching energy, leading to small redshifts or at least no blueshifts in the C—H vibrations of the cationic 2-ME. The presence of two oxygen atoms in the 2-ME molecule may account for these findings, as negative hyperconjugation occurs between the $C_\alpha H$ bonds and the nonbonding orbital of the oxygen atoms. This delocalizes the nonbonding n(O) electrons into the $C_\alpha H$ bonds. To further investigate this phenomenon, a Natural Bond Orbital (NBO) calculation of neutral 2-ME (gG′T) was performed at the B3LYP/def2-TZVPP level (pop=nboread). As depicted in Fig. (5b-c), a significant overlap was observed between the n(O1) orbital and the two neighboring σ* bond orbitals (C3-H6 and C5-H12). A similar strong interaction was also observed between the n(O2) orbital and the neighboring σ*(C4-H8) orbitals, as shown in Fig. (5d). Table 2

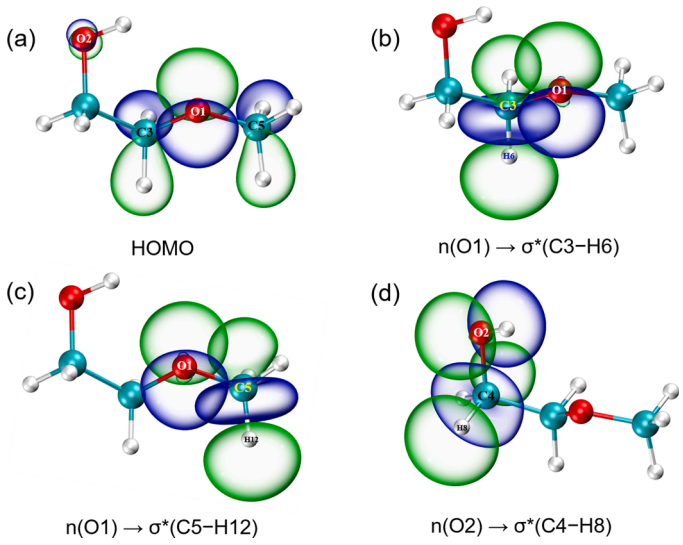

Fig. 5. The calculated electron density distribution of the HOMO in neutral 2-ME (Fig. 5a) and the overlap between the n(O) and σ*(C—H) orbitals illustrated by the natural bond orbital (NBO) plots (Fig. 5b-d). The calculation was conducted at the B3LYP/def2-TZVPP level (pop=nboread). The isodensity surface is depicted at the value of 0.05.

Table 2
Second-order perturbation Energy E(2) (kcal mol^{-1}) for the intramolecular interactions in the gG′T conformer of neutral 2-ME.

Conformer	Type of interaction	E(2)
neutral (gG′T)	n(O1) → σ*(C3−H6)	7.85
	n(O1) → σ*(C3−H7)	6.19
	n(O1) → σ*(C5−H11)	6.74
	n(O1) → σ*(C5−H12)	7.06
	n(O1) → σ*(C5−H10)	2.24
	n(O2) → σ*(C4−H9)	2.28
	n(O2) → σ*(C4−H8)	7.86

a Only the interactions between C—H and n(O) electrons with energies greater than 2 kcal mol^{-1} are listed in the table.

presents the second-order perturbation energies (E(2)), which serve as indicators of the extent of electron delocalization through hyperconjugation, between the nonbonding n(O1 and O2) orbitals and the bonding σ*(C_αH) orbitals (only E(2) values greater than 2 kcal mol^{-1} are listed in the table). The E(2) values for the n(O1)→σ*(C3−H6), n(O1)→σ*(C5−H12), and n(O2)→σ*(C4−H8) interactions are 7.85, 7.06 and 7.86 kcal mol^{-1}, respectively. Consequently, negative hyperconjugation weakens the CαH bonds, resulting in a further decrease in the vibrational frequency of the C-H, similar to what is observed in tetrahydrofuran (THF) and tetrahydropyran (THP) molecules [55]. Previous studies have demonstrated that the negative hyperconjugation of n(O)→σ*(C_αH) in the neutral state can transition to the positive hyperconjugation of σ(C_αH)→n*(O) upon ionization, thereby weakening the cationic C_αH bonds [55]. However, no significant σ(C_αH)→n*(O) interaction was observed in cationic 2-ME through the second-order perturbation analysis (with a threshold of 0.5 kcal mol^{-1}) using the NBO calculation.

In summary, while the removal of electrons from the HOMO has minimal impact on the C—H bonds, the NBO analysis revealed that the strong negative hyperconjugation resulting from the n(O)→σ*(C_αH) interactions weakens the C_αH bonds in neutral 2-ME. This phenomenon leads to a blueshift of approximately 100 cm^{-1} in the C-H stretching frequencies of cationic 2-ME compared to neutral 2-ME.

4. Conclusions

In summary, the dominant conformer and IR spectra of neutral and cationic 2-ME in the gas phase were obtained using the IR−VUV NRIFD-IR method. Quantum chemical calculations revealed that the gG′T, stabilized by an intramolecular hydrogen bond (OH···O), is the most stable conformer of neutral 2-ME. This conformer was found to be the primary carrier of the IR spectrum, as the simulated IR spectra showed better agreement with the experimental results. The three prominent features observed were assigned to the CH stretching fundamental mode (ν_{CH}), the OH stretching fundamental mode (ν_{OH}), and the OH first overtone mode ($2\nu_{OH}$).

The most stable conformer of cationic 2-ME exhibited significant structural changes compared to the neutral 2-ME. The IRI map analysis indicated that although the O-H···O intramolecular hydrogen bond was disrupted upon ionization, a weak C-H···O hydrogen bond was formed, which played a crucial role in stabilizing the cationic species. The simulated IR spectra of the C2 conformer showed better agreement with the experimental spectra, particularly in the CH stretching region, compared to the C1 conformer.

The measured IR spectra show that the C-H fundamental stretching mode of cationic 2-ME is blue-shifted by about 100 cm^{-1} compared to that of neutral 2-ME. This observation aligns with the findings from the NBO analysis, which revealed that in neutral 2-ME, the n(O)→σ*(C_αH) interactions result in significant negative hyperconjugation, leading to a weakening of the C_αH bonds. Consequently, the C-H stretch of neutral 2-ME experiences a redshift relative to that of cationic 2-ME.

The present work highlights the critical role of intramolecular hydrogen bonds in stabilizing both neutral and cationic species. Moreover, it provides an illustrative example of the substantial structural changes between neutral and corresponding cationic species upon breaking the O-H···O intramolecular hydrogen bond following ionization.

CRediT authorship contribution statement

Xiaohu Zhou: Conceptualization, Data curation, Formal analysis, Methodology, Writing – original draft. **Ende Huang:** Conceptualization, Data curation, Methodology. **Licheng Zhong:** Data curation, Methodology. **Siyue Liu:** Data curation, Methodology. **Shuze Ma:** Data curation, Methodology. **Hongwei Li:** Data curation, Methodology. **Xueming Yang:** Project administration, Supervision, Resources, Visualization. **Wenrui Dong:** Conceptualization, Funding acquisition, Methodology, Project administration, Supervision, Validation, Visualization, Resources, Writing – review & editing.

Declaration of Competing Interest

The authors declare that they have no known competing financial interests or personal relationships that could have appeared to influence the work reported in this paper.

Data availability

Data will be made available on request.

Acknowledgments

The authors gratefully acknowledge the Dalian Coherent Light Source (DCLS) for support and assistance. This work was funded by the National Natural Science Foundation of China (NSFC No. 22288201), the Chinese Academy of Sciences (GJJSTD20220001), and the Innovation Program for Quantum Science and Technology (No.2021ZD0303305).

Supplementary materials

Supplementary material associated with this article can be found, in the online version, at doi:10.1016/j.molstruc.2023.136389.

References

[1] T. Steiner, The hydrogen bond in the solid state, Angew. Chem., Int. Ed. 41 (2002) 48–76.
[2] C.L. Perrin, J.B. Nielson, Strong" hydrogen bonds in chemistry and biology, Annu. Rev. Phys. Chem. 48 (1997) 511–544.
[3] I. Alkorta, I. Rozas, J. Elguero, Non-conventional hydrogen bonds, Chem. Soc. Rev. 27 (1998) 163–170.
[4] L.P. Kuh, The hydrogen bond. I. Intra- and intermolecular hydrogen bonds in alcohols, J. Am. Chem. Soc. 74 (1952) 2492–2499.
[5] R.L. Brinkley, R.B. Gupta, Intra- and intermolecular hydrogen bonding of 2-methoxyethanol and 2-butoxyethanol in n-hexane, Ind. Eng. Chem. Res. 37 (1998) 4823–4827.
[6] M.H. Abraham, R.J. Abraham, A.E. Aliev, C.F. Tormena, Is there an intramolecular hydrogen bond in 2-halophenols? A theoretical and spectroscopic investigation, Phys. Chem. Chem. Phys. 17 (2015) 25151–25159.
[7] E.E. Fileti, P. Chaudhuri, S. Canuto, Relative strength of hydrogen bond interaction in alcohol–water complexes, Chem. Phys. Lett. 400 (2004) 494–499.
[8] F.A.J. Singelenberg, J.H. van der Maas, An FT-IR study on intramolecular hydrogenbonding in ethylene glycol derivatives, J. Mol. Struct. 245 (1991) 183–194.
[9] H.E. Audier, A. Milliet, D. Leblanc, T.H. Morton, Unimolecular decompositions of the radical cations of ethylene glycol and its monomethyl ether in the gas phase. Distonic ions versus ion-neutral complexes, J. Am. Chem. Soc. 114 (1992) 2020–2027.
[10] H. Yoshida, K. Takikawa, K. Ohno, H. Matsuura, Vibrational spectroscopic study of 2-methoxyethanol: matrix-isolation infrared spectra and conformational analysis based on ab initio mo calculations, J. Mol. Struct. 299 (1993) 141–147.

[11] F.P.S.C. Gil, R. Fausto, A.M. Amorim da Costa, J.J.C. Teixeira-Dias, Structures and vibrational spectra of $CH_3OCH_2CH_2OH$: the hydrogen-bonded conformers, J. Chem. Soc., Faraday Trans. 90 (1994) 689–695.

[12] F.P.S.C. Gil, J.J.C Teixeira-Dias, Structures and vibrational spectra for the conformers of $CH_3OCH_2CH_2OH$, J. Mol. Struct. (Theochem) 332 (1995) 269–275.

[13] M. Buck, Ab initio calculations of vibrational spectra of 2-methoxy ethanol in the C-H stretching range, Phys. Chem. Chem. Phys. 5 (2003) 18–25.

[14] M. Gawrilow, M.A. Suhm, 2-methoxyethanol: harmonic tricks, anharmonic challenges and chirality-sensitive chain aggregation, Phys. Chem. Chem. Phys. 22 (2020) 15303–15311.

[15] Z. Jiang, Y. Liu, T. Jing, B. Huang, Z. Wang, X. Zhang, X. Qin, Y. Dai, Enhancing visible light photocatalytic activity of TiO_2 using a colorless molecule (2-methoxyethanol) due to hydrogen bond effect, Appl. Catal. B 200 (2017) 230–236.

[16] J.W. Yoo, J. Jang, U. Kim, Y. Lee, S.-G. Ji, E. Noh, S. Hong, M. Choi, S.I. Seok, Efficient perovskite solar mini-modules fabricated via bar-coating using 2-methoxyethanol-based formamidinium lead tri-iodide precursor solution, Joule 5 (2021) 2420–2436.

[17] D.-K. Lee, D.-N. Jeong, T.K. Ahn, N.-G. Park, Precursor engineering for a large-area perovskite solar cell with >19% efficiency, ACS Energy Letters 4 (2019) 2393–2401.

[18] X. Dai, Y. Deng, C.H. Van Brackle, S. Chen, P.N. Rudd, X. Xiao, Y. Lin, B. Chen, J. Huang, Scalable fabrication of efficient perovskite solar modules on flexible glass substrates, Adv. Energy Mater. 10 (2020), 1903108.

[19] L. Guo, Y. Chen, G. Wang, Y. Xia, D. Luo, Z. Zhu, C. Wang, W. Dong, S. Wen, Efficient perovskite solar cells achieved using the 2-methoxyethanol additive: morphology and composition control of intermediate film, ACS Appl. Energy Mater. 4 (2021) 2681–2689.

[20] G. Li, Y.Y. Zhang, Q. Li, C. Wang, Y. Yu, B. Zhang, H.S. Hu, W. Zhang, D. Dai, G. Wu, D.H. Zhang, J. Li, X. Yang, L. Jiang, Infrared spectroscopic study of hydrogen bonding topologies in the smallest ice cube, Nat. Commun. 11 (2020) 5449.

[21] M. Miyazaki, A. Fujii, T. Ebata, N. Mikami, Infrared spectroscopic evidence for protonated water clustersforming nanoscale cages, Science 304 (2004) 1134–1137.

[22] H.L. Han, C. Camacho, H.A. Witek, Y.-P. Lee, Infrared absorption of methanol clusters $(CH_3OH)_n$ with n = 2-6 recorded with a time-of-flight mass spectrometer using infrared depletion and vacuum-ultraviolet ionization, J. Chem. Phys. 134 (2011), 144309.

[23] H.B. Fu, Y.J. Hu, E.R. Bernstein, IR + vacuum ultraviolet (118nm) nonresonant ionization spectroscopy of methanol monomers and clusters: neutral cluster distribution and size-specific detection of the OH stretch vibrations, J. Chem. Phys. 124 (2006), 024302.

[24] Y. Matsuda, M. Mori, M. Hachiya, A. Fujii, N. Mikami, Infrared spectroscopy of size-selected neutral clusters combined with vacuum-ultraviolet-photoionization mass spectrometry, Chem. Phys. Lett. 422 (2006) 378–381.

[25] M. Katada, R. Shishido, A. Fujii, Infrared spectroscopy of large-sized neutral and protonated ammonia clusters, Phys. Chem. Chem. Phys. 16 (2014) 7595–7601.

[26] Y. Matsuda, K. Hoki, S. Maeda, K. Hanaue, K. Ohta, K. Morokuma, N. Mikami, A. Fujii, Experimental and theoretical investigations of isomerization reactions of ionized acetone and its dimer, Phys. Chem. Chem. Phys. 14 (2012) 712–719.

[27] J. Guan, Y. Hu, M. Xie, E.R. Bernstein, Weak carbonyl-methyl intermolecular interactions in acetone clusters explored by IR plus vuv spectroscopy, Chem. Phys. 405 (2012) 117–123.

[28] J.Y. Feng, Y.P. Lee, C.Y. Zhu, P.J. Hsu, J.L. Kuo, T. Ebata, IR-vuv spectroscopy of pyridine dimers, trimers and pyridine-ammonia complexes in a supersonic jet, Phys. Chem. Chem. Phys. 22 (2020) 21520–21534.

[29] T. Lu, Molclus Program 2022, Beijing Kein Research Center for Natural Science, China, 2022. http://www.keinsci.com/research/molclus.html.

[30] S. Grimme, J. Antony, S. Ehrlich, H. Krieg, A consistent and accurate ab initio parametrization of density functional dispersion correction (DFT-D) for the 94 elements H-Pu, J. Chem. Phys. 132 (2010), 154104.

[31] M. Sierka, A. Hogekamp, R. Ahlrichs, Fast evaluation of the coulomb potential for electron densities using multipole accelerated resolution of identity approximation, J. Chem. Phys. 118 (2003) 9136–9148.

[32] S. Grimme, S. Ehrlich, L. Goerigk, Effect of the damping function in dispersion corrected density functional theory, J. Comput. Chem. 32 (2011) 1456–1465.

[33] G.W.T.M.J. Frisch, H.B. Schlegel, G.E. Scuseria, M.A. Robb, J.R. Cheeseman, G. Scalmani, V. Barone, G.A. Petersson, H. Nakatsuji, X. Li, M. Caricato, A. V. Marenich, J. Bloino, B.G. Janesko, R. Gomperts, B. Mennucci, H.P. Hratchian, J. V. Ortiz, A.F. Izmaylov, J.L. Sonnenberg, D. Williams-Young, F. Ding, F. Lipparini, F. Egidi, J. Goings, B. Peng, A. Petrone, T. Henderson, D. Ranasinghe, V. G. Zakrzewski, J. Gao, N. Rega, G. Zheng, W. Liang, M. Hada, M. Ehara, K. Toyota, R. Fukuda, J. Hasegawa, M. Ishida, T. Nakajima, Y. Honda, O. Kitao, H. Nakai, T. Vreven, K. Throssell, J.A. Montgomery Jr., J.E. Peralta, F. Ogliaro, M. J. Bearpark, J.J. Heyd, E.N. Brothers, K.N. Kudin, V.N. Staroverov, T.A. Keith, R. Kobayashi, J. Normand, K. Raghavachari, A.P. Rendell, J.C. Burant, S.S. Iyengar, J. Tomasi, M. Cossi, J.M. Millam, M. Klene, C. Adamo, R. Cammi, J.W. Ochterski, R.L. Martin, K. Morokuma, O. Farkas, J.B. Foresman, D.J. Fox, Gaussian 16, Revision A.03, Gaussian Inc., Wallingford, CT, 2016.

[34] F. Neese, The ORCA program system, WIREs Comput. Mol. Sci. 2 (2011) 73–78.

[35] T. Lu, F. Chen, Multiwfn: a multifunctional wavefunction analyzer, J. Comput. Chem. 33 (2012) 580–592.

[36] W. Humphrey, A. Dalke, K. Schulten, VMD: visual molecular dynamics, J. Mol. Graph. 14 (1996) 33–38.

[37] M.A. Abdel-Rahman, T.M. El-Gogary, N. Al-Hashimi, M.F. Shibl, K. Yoshizawa, A. M. El-Nahas, Computational studies on the thermodynamic and kinetic parameters of oxidation of 2-methoxyethanol biofuel via H-atom abstraction by methyl radical, Sci. Rep. 9 (2019) 15361.

[38] T. Lu, Q. Chen, Interaction region indicator: a simple real space function clearly revealing both chemical bonds and weak interactions**, Chem.-Methods 1 (2021) 231–239.

[39] F.P. Lossing, Heats of formation of some isomeric $[C_nH_{2n+1}O]^+$ ions. Substitutional effects on ion stability, J. Am. Chem. Soc. 99 (1977) 7526–7530.

[40] K. Kimura, S. Katsumata, Y. Achiba, T. Yamazaki, S. Iwata, Handbook of HeI Photoelectron Spectra of Fundamental Organic Molecules: Ionization energies, Ab Initio assignments, and Valence Electronic Structure for 200 Molecules, Japan Scientific Societies Press, Tokyo, 1981.

[41] H. Zhan, Y. Hu, P. Wang, J. Chen, Dominant conformer of tetrahydropyran-2-methanol and its clusters in the gas phase explored by the use of vuv photoionization and vibrational spectroscopy, J. Chem. Phys. 146 (2017), 134303.

[42] E.R. Johnson, S. Keinan, P. Mori-Sanchez, J. Contreras-Garcıa, A.J. Cohen, W. T. Yang, Revealing noncovalent interactions, J. Am. Chem. Soc. 132 (2010) 6498–6506.

[43] H. Yoshida, T. Harada, K. Ohno, H. Matsuura, Infrared spectroscopic evidence for an attractive intramolecular 1,5-CH···O interaction in 1-methoxy-2-(methylthio) ethane, Chem. Commun. (1997) 2213–2214.

[44] S. Tsuzuki, T. Uchimaru, K. Tanabe, Conformational analysis of 1,2-dimethoxy-ethane by ab initio molecular orbital and molecular mechanics calculations: stabilization of the TGG' rotamer by the 1,5 CH_3/O nonbonding attractive interaction, J. Phys. Chem. 97 (1993) 1346–1350.

[45] H. Yoshida, T. Harada, T. Murase, K. Ohno, H. Matsuura, Conformational stabilization by intramolecular OH···S and CH···O interactions in 2-(methylthio) ethanol. Matrix-isolation infrared spectroscopy and ab initio mo calculations, J. Phys. Chem. A 101 (1997) 1731–1737.

[46] T. Harada, H. Yoshida, K. Ohno, H. Matsuura, Implications of intramolecular OH···Se hydrogen bonding and CH···O interaction in the conformational stabilization of 2-(methylseleno)ethanol studied by vibrational spectroscopy and density functional theory, J. Phys. Chem. A 105 (2001) 4517–4523.

[47] J.L. Holmes, F.P. Tossing, The radical cation $[CH_2OH_2]^{+\cdot}$ and related stable gas-phase ion-dipole complexes, J. Am. Chem. Soc. 104 (1982) 2931–2932.

[48] P.C. Burgers, J.L. Holmes, J.K. Terlouw, B. van Baar, Three new isomers of $[C_2H_6O]^{+\cdot}$: the radical cations $[CH_3O(H)CH_2]^{+\cdot}$, $[CH_3CHOH_2]^{+\cdot}$ and a low-energy isomer of unassigned structure, Org, Mass Spectrom 20 (1985) 202–206.

[49] T.H. Morton, Gas phase analogues of solvolysis reactions, Tetrahedm 38 (1982) 3195–3243.

[50] H.W. Biermann, T.H. Morton, Reversible tautomerization of radical cations. Photoionization of 2-methoxyethanol and 3-methoxy-1-propanol, J. Am. Chem. Soc. 105 (1983) 5025–5030.

[51] C.C. Van de Sande, F.W. McLafferty, The structure and formation of stable $C_3H_6O^+$ ions, J. Am. Chem. Soc. 97 (1975) 4617–4620.

[52] J.L. Holmes, F.P. Lossing, Heats of formation of organic radicals from appearance energies, Int. J. Mass Spectrom. Ion Processes 58 (1984) 113–120.

[53] Y.J. Hu, H.B. Fu, E.R. Bernstein, Infrared plus vacuum ultraviolet spectroscopy of neutral and ionic ethanol monomers and clusters, J. Chem. Phys. 125 (2006), 154305.

[54] Y.J. Hu, H.B. Fu, E.R. Bernstein, IR plus vacuum ultraviolet spectroscopy of neutral and ionic organic acid molecules and clusters: acetic acid, J. Chem. Phys. 125 (2006), 184308.

[55] M. Xie, Y. Matsuda, A. Fujii, Infrared spectroscopic investigation of photoionization-induced acidic C-H bonds in cyclic ethers, J. Phys. Chem. A 119 (2015) 5668–5675.

[56] A. Rauk, T.S. Sorensen, C. Maerker, J.W. de M. Carneiro, S. Sieber, P. v. R. Schleyer, Axial, and equatorial 1-methyl-1-cyclohexyl cation isomers both have chair conformations but differ in C-C and C-H hyperconjugation modes, J. Am. Chem. Soc. 118 (1996) 3761–3762.

[57] T. Leyssens, D. Peeters, Negative hyperconjugation in phosphorus stabilized carbanions, J. Org. Chem. 73 (2008) 2725–2730.

[58] A.E. Reed, P.v.R. Schleyer, Chemical bonding in hypervalent molecules. The dominance of ionic bonding and negative hyperconjugation over d-orbital participation, J. Am. Chem. Soc. 112 (1990) 1434–1445.

[59] Y.R. Mo, Y.Q. Zhang, J.L. Gao, A simple electrostatic model for trisilylamine: theoretical examinations of the $n\rightarrow\sigma^*$ negative hyperconjugation, $p_\pi\rightarrow d_\pi$ bonding, and stereoelectronic interaction, J. Am. Chem. Soc. 121 (1999) 5737–5742.

[60] T.A. Beu, U. Buck, Vibrational spectra of ammonia clusters from n=3 to 18, J. Chem. Phys. 114 (2001) 7853–7858.